IEEE Access
Multidisciplinary | Rapid Review | Open Access Journal

Received 30 October 2024, accepted 18 December 2024, date of publication 26 December 2024, date of current version 6 January 2025.

Digital Object Identifier 10.1109/ACCESS.2024.3523292

RESEARCH ARTICLE

Motion Classification With Embroidery Bend Sensors Using Multiple Zigzag-Stitch for Loose-Fitting Garments

KAISEI MINAMI, YASUHIRO AKIYAMA, (Member, IEEE), AND TAKUYA UMEDACHI
Faculty of Textile Science and Technology, Shinshu University, Nagano 390-8621, Japan

Corresponding author: Kaisei Minami (23fs323d@shinshu-u.ac.jp)

This work was supported by KAKENHI (Grant-in-Aid for Scientific Research (B)) [Grant Number 21H01289] from the Japan Society for the Promotion of Science (JSPS) and by Chuo Electronics Company Ltd.

This work involved human subjects or animals in its research. Approval of all ethical and experimental procedures and protocols was granted by the Ethics Committee of the Shinshu University under Application No. 387.

ABSTRACT This study proposes a wearable motion classification system by employing commercially available conductive threads and everyday garments. The unique feature of the proposed system is an embroidery bending sensor that does not necessitate tight-fitting with the body, which contrasts with traditional motion sensing systems. Therefore, integration can be simplified by allowing motion classification onto loose-fitting everyday garments. The sensor that exhibits a change in resistance to bending deformation is realized by applying multiple zigzag stitch to the fabric. In addition, a significant resistance change is realized during the phase transition of motions (e.g., stance and swing phase). Therefore, motion can be categorized without making joint angle measurements. We fabricated a prototype by attaching the sensors to a commercially available work jacket and pants by sewing them onto the fabric. Ten participants were requested to perform ten various activities (e.g., walking, jogging, ascending and descending stairs). The findings demonstrated that the sensor can measure the degree of joint flexion, the flexion cycle, and the timing of flexion during the wearer's activities. Moreover, motion classification was performed by training a one-dimensional convolutional neural network (1D-CNN) model with the sensor signals. The model successfully learned the differences in signal amplitude and frequency as distinguishing features of each activity, resulting in an average classification accuracy of 99.02% across the ten types of activities.

INDEX TERMS Flexible sensors, loose-fitting garments, motion classification, machine learning, smart textiles, wearable sensors.

I. INTRODUCTION

Monitoring and analyzing human motion allows us to obtain useful information, such as health records, injury prevention, risk assessment, and evaluation of posture and motion patterns. Detecting gait disturbance due to neurological causes such as dementia or Parkinson's disease is possible by monitoring gait motion [1]. In addition, the changes in health status and physical functions of the elderly can be recorded and detected regularly by monitoring their motions [2]. Therefore, better health management, safety assurance, and early symptom detection and intervention can be achieved. By monitoring the activities of factory workers, abnormal movements can also be detected and early warnings of potential malfunctions can be provided, thereby preventing industrial accidents [3].

Motion sensing using a wearable device is an effective means of monitoring in any environmental setup. This is because wearable devices are designed for non-invasive and continuous environmental monitoring of the aforementioned activities. Therefore, several methods such as employing accelerometers placed inside garments and performing Fast

The associate editor coordinating the review of this manuscript and approving it for publication was Ajit Khosla.

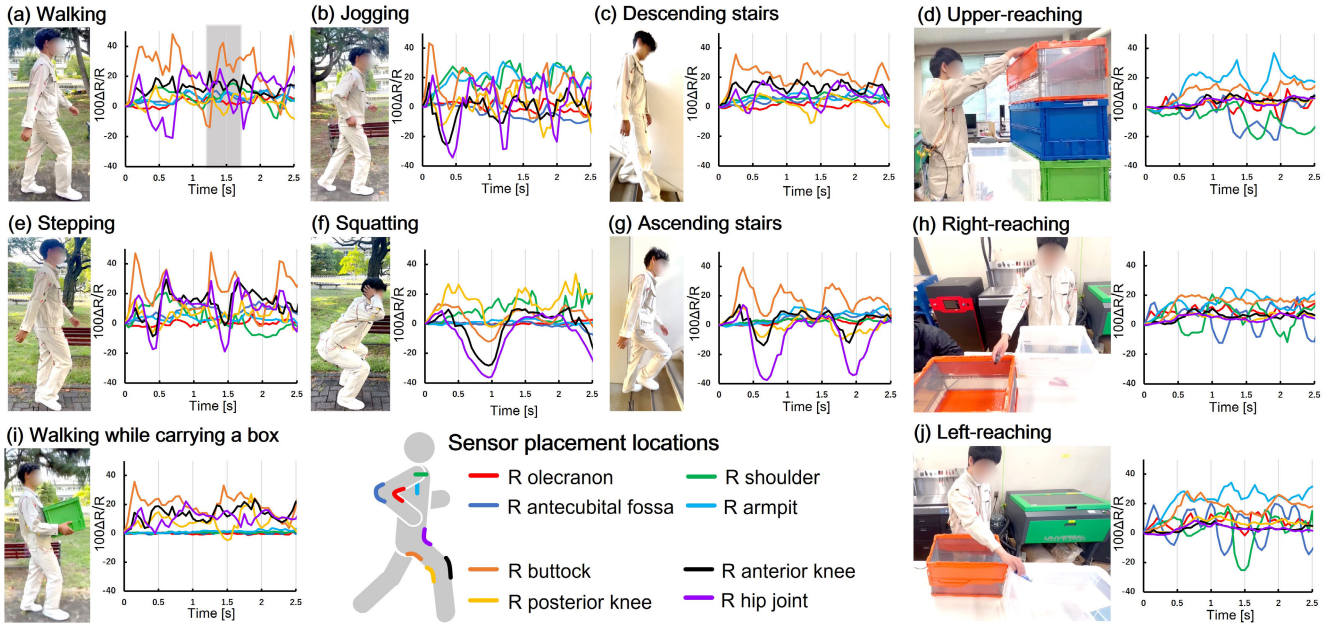

FIGURE 1. Activities classified in this study and their corresponding signals.

Fourier Transforms (FFTs) on the measured data [4], [5], and using inertial sensors [6], [7], [8] have been developed for sensing body motion. Although these systems provide high accuracy, the sensors must be fixed to a body part. In addition, rigid sensors placed around joints increase user discomfort.

Attaching flexible sensors directly to a garment has been proposed by several researchers/engineers. Specifically, for sensing methods based on strain [16], [17], [18], [19] and pressure sensors [20], [21], where stretching deformation of the garments leads to a change in resistance. Therefore, these techniques work only on tight garments. Hence, pressure sensor, which is attached to a band or garments, monitors muscle activity and requires tight contact between the sensor(s) and the body.

In this study, we propose a sensor system capable of classifying the wearer's activities by attaching an embroidered bending sensor fabricated using a conventional sewing machine and conductive thread to loose-fitting clothing. In addition, this sensor is realized by applying a multiple zigzag stitch to the fabric. The sensor is crafted by stitching the conductive thread onto the locations where the garment undergoes bending deformation. The resistance of the sensor changes in response to the motion of the wearer. We designed the multiple zigzag stitch to classify motions rather than measure joint angles. Thus, this sensor exhibits a significant change in resistance during the phase transition of motions (e.g., stance and swing phase). By inputting the time-series data of the sensor's resistance changes into deep learning models, the system can learn the signal characteristics of each activity to enable motion classification. These characteristics include the degree and timing of joint flexion in the arms and legs. The contributions of this study are summarized as follows:

- We developed a sensor that exhibits changes in resistance in response to bending deformation by applying multiple zigzag stitch with conductive thread onto fabric.
- We placed the sensor at 16 locations on a commercially available loose-fitting work outfit (jacket and pants) and proposed a sensor system to classify the wearer's activities.
- We evaluated the proposed method via an experiment involving ten participants. Ten different activities (walking, walking while carrying a box, jogging, stepping, squatting, ascending and descending stairs, upward-reaching, left-reaching, and right-reaching) were classified.
- We applied a one-dimensional CNN model to the collected data and, achieved an average accuracy of 99.02% (SD: 0.19) by employing 5-fold cross-validation.

II. RELATED WORKS

A. SENSING WITH LOOSE-FITTING GARMENTS

Related methods of attaching sensors to loose-fitting garments are based on capacitive [15], triboelectric [11], and piezoelectric sensors [14]. These methods are effective in motion classification. However, the following problems deter their practicability; the sensor can be used only in limited environments, the production method is complex, and the wearer's comfort is compromised. In addition, the capacitive sensors [22] do not function in the presence of metallic objects nearby. Triboelectric sensors employ complex fabrication processes, which require many fabrication processes for garments. Moreover, the stiff film of the piezoelectric sensor attached to a garment causes discomfort to the user. It is worth noting that the stiffness distribution of the

TABLE 1. Comparison of methods for activity classification using loose-fitting clothing.

Studies	Device	Activities	Accuracy	Persons
Shirt:Digital Electronic [9]	Flexible fiber: 100 microchips with temperature sensing	4 motor activities	96.40 %	1
Jacket and pant [10]	Hetero-core fiber optics	8 motor activities	98.70 %	1
Sleeve [11]	Fabric-based triboelectric joint sensing	4 daily activities	91.30 %	14
RFID system [12]	4 antennas; back, chest and feet	5 motor + 3 cleaning activities	93.60 %	4
Sweat jacket [13]	Optical-strain sensor	5 motor activities	90.90 %	12
Loose Pants [14]	Flexible piezoelectric	5 motor activities + 8 transitions	93.00 %	10
MoCapaci [15]	Textile cables as capacitive antennas	20 posture/gestures	97.18 %	14
Our approach	Embroidery bend sensor	10 motor activities	99.02 %	10

fabric changes significantly. Therefore, the more sensors are attached to the garments, the more discomfort may be experienced by the user.

Table 1 compares previous approaches toward sensors employed in clothing. While many methods employ complex sensing principles that are difficult to integrate into e-textile components, our proposed system has developed an embroidered-type flex sensor that can be manufactured using a standard sewing machine and conductive thread. The sensor employs a resistive method, simplifying the measurement circuit, and it can be easily incorporated into commercially available fabrics by sewing in a conductive thread.

B. EMBROIDERY SENSOR SYSTEM USING CONDUCTIVE THREAD

Pressure, elongation, and bending sensors are being pursued as wearable sensors that can be sewn via conductive threads into textile material.

Moreover, pressure sensors have been proposed to be sewn into non-conductive fabrics [23], conductive fabrics [24], or capacitive types [25]. However, these sensors are characterized as interface devices to input the user's commands and are not designed as body motion sensing devices. Therefore, the sensor must be in close contact with the wearer's skin and firmly fixed to detect motion.

Elongation sensors are fabricated using various sewing methods such as zigzagstitch, coverstitch, and overlockstitch. The change in resistance in response to the elongation of the fabric has been evaluated [26], [27], [28]. Some studies have shown that it is possible to measure joint angles using the coverstitch [29], [30]. The accuracy of the motion analysis using this method is high; however, it must be incorporated into a tight garment because of the need to generate elongation deformation in the garment.

Fabrication using the coverstitch method has been proposed for bending sensors. The possibility of measuring the angle of the joint has been investigated by sewing the sensor into the section of the jeans where bending and stretching of the knee causes bending deformation [31]. However, the coverstitch is a complicated sewing method using multiple needles and requires a special machine. Therefore, in this study, we propose an improved stitch pattern and a method to analyze the time-series change of resistance for easy motion classification.

III. EMBROIDERY BEND SENSOR

A. CONCEPT OF THE PROPOSED SENSOR

The proposed sensor utilizes the multiple zigzag-stitch (in this study we use triple zigzag) [32]. Fig. 2(a) shows a schematic of the triple zigzag stitch. The bundle segment is drawn to stitch a thread back and forth 1.5 times. The proposed stitching creates electrical short paths at corners and bundles. Bending deformation causes a change in the contacts between the thread at the bundle and the corner sections (Fig. 2(a)), resulting in a change in the resistance value. This significantly differs from the usual zigzagstitch in which the thread is stitched once to form a bundle section. Here, φ denotes the curvature of the sensor. When the sensor is bent in the direction of tensile strain on the conductive thread side, $\varphi > 0$ (Fig. 2(b–c)). When bending in the direction of the compressive strain on the conductive thread side, $\varphi < 0$ (Fig. 2(d–e)).

Employing multiple zigzag-stitch enables us to adjust the thread consumption and sensor sensitivity by changing the stitch width (p) and the pretend width (w), as shown in Fig. 2. p and w can be changed independently; however, in this section, we discuss the sensor performance by changing θ, which is the half angle of the zigzag line corner. θ can be determined as follows:

$$\theta = \arctan \frac{p}{2w}. \tag{1}$$

A change in θ affects the rate of change of the sensor's resistance. This is because the number of bundle sections N per fixed length of the sensor and the number of corner

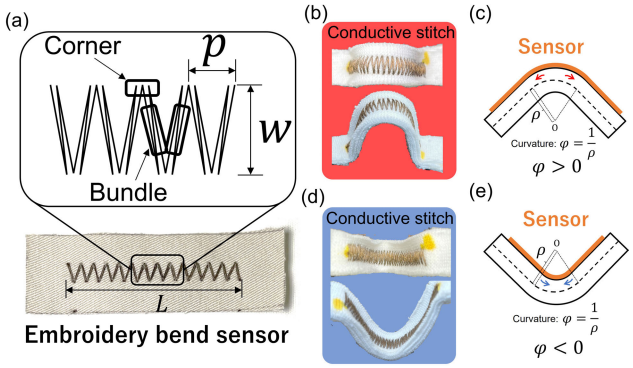

FIGURE 2. (a) Embroidery bend sensor and details of its stitching. (b–e) Types of bending deformation.

sections $N-1$ vary with θ, as follows:

$$N = \frac{L}{p/2} = \frac{L}{w\tan\theta}, \tag{2}$$

where L denotes the sensor length.

B. HOW TO FABRICATE THE SENSOR

The conductive thread used in this study is a Smart-X #50 (Fujix, Inc.), whose elongation capability is 35%. This thread is manufactured from silver-plated nylon 66 fiber and has sufficient conductivity (line resistance: approx. 250 Ωm^{-1}) and wash durability [33].

Two steps are involved in the sensor fabrication process. The first step is to design a triple zigzag-stitch using the embroidery production software Tajima Writer PLUS (Fig. 3(a)). The second step is to sew the design into the fabric using a Tajima SAI (Tajima Industries, Inc.) embroidery machine (Fig. 3(b)). In this study, the upper thread is conductive, whereas the lower thread is nonconductive.

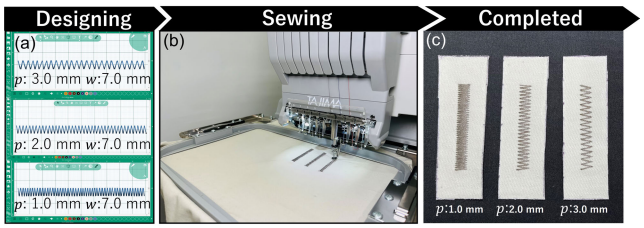

FIGURE 3. Procedure for fabrication of embroidery bend sensors.

C. BENDING EXPERIMENT WITH A SINGLE SENSOR

1) EXPERIMENTAL SETUP

Sensors with different θ values were fabricated, and the change in the resistance was measured when the seams on the conductive thread side were subjected to tensile and compressive deformation. First, three sensors were fabricated with the seam fixed at $w = 7$ mm and varied in the range of 1 mm $\leq p \leq$ 3 mm (p in 1 mm increments).

A robotic arm (UR3e; Universal Robots) was used to continuously change the bending curvature of the sensor in the following manner. One end of the sensor was fixed, whereas the other end was attached to the end effector of the robotic arm (Fig. 4(a)). Next, the sensor was deformed by sliding the robotic arm (Fig. 4(b–c)). This sliding motion is performed five times, bending and returning to the original position for 2 s and stopping for 2 s. The change in the resistance was measured using an Arduino Mega 2560.

The change in bending curvature of the sensor was measured using a two-dimensional motion analysis application (Kinovea). The range of the length of the sensor with varying curvature was set to 20 mm. In addition, three markers were placed at both ends and in the middle of the sensor (Fig. 4(b)). The bending curvature was assumed to be constant in that section. Then, we filmed a video of the sensor bending curvature changing, tracked the coordinates of the three markers using Kinovea, and calculated the bending curvature of the circle passing through the three points (Fig. 4(c)).

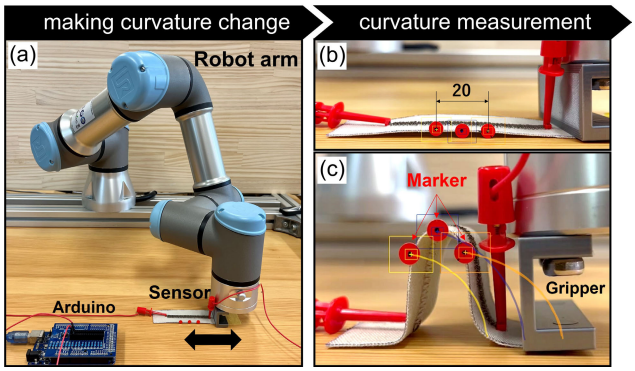

FIGURE 4. Bending experiment procedure.

2) EXPERIMENTAL RESULTS

Fig. 5(a, c, e) and (b, d, f) shows the resistance changes when $\varphi > 0$ and $\varphi < 0$, respectively. The resistance changes of the sensor initially increased and then decreased as the bending curvature increased. In addition, we confirmed that the resistance value increased and then decreased when the bending of the sensor was resolved, which will be discussed in Section V-A.

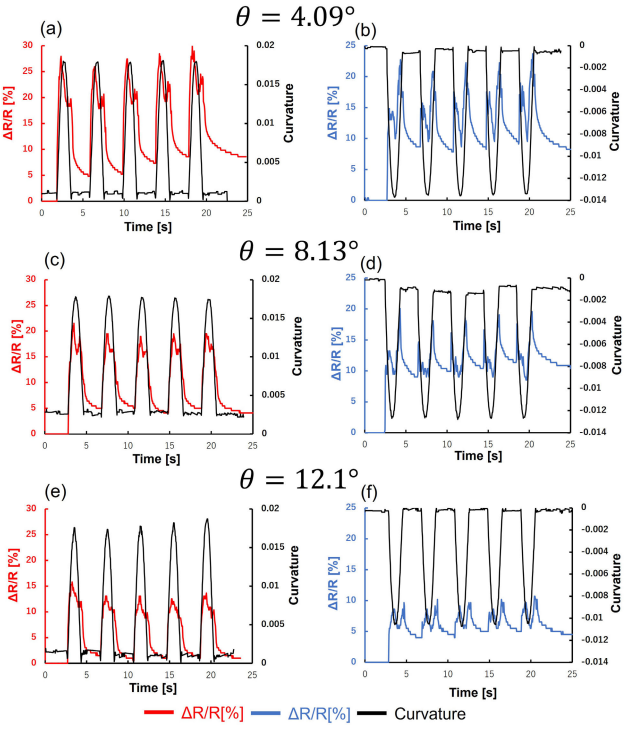

FIGURE 5. Relationship between sensor bending curvature and resistance during deformation for (a, c, e) $\varphi > 0$ and (b, d, f) $\varphi < 0$.

The range of the resistance change increased when the value of θ decreased: the wider range of the resistance change

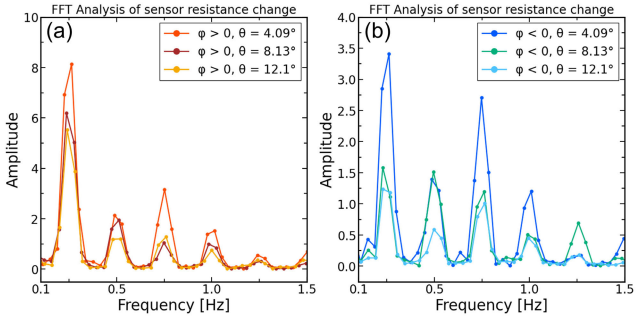

FIGURE 6. FFT analysis of the sensor's resistance change: (a) $\varphi > 0$, (b) $\varphi < 0$.

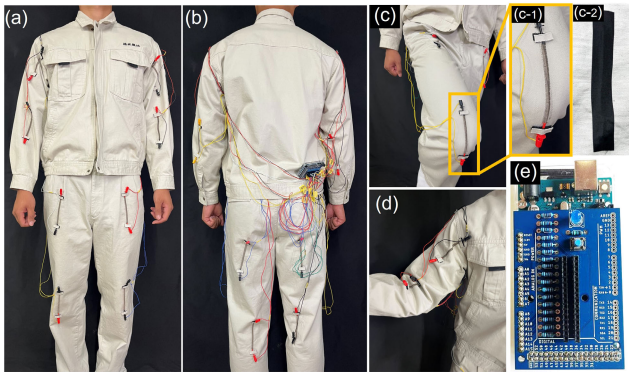

FIGURE 7. (a, b) Overall view of the prototype. (c, d) Deformation of the sensor during the wearer's motion and the surface (c-1) and wrong side (c-2) of the mounted sensor. (e) Prototype of the resistance value measurement device.

can be achieved when $\theta = 4.09$. Fig. 6 shows the FFT analysis results. The results show that the largest amplitude can be achieved when $\theta = 4.09$ in cases of $\varphi > 0$ and $\varphi < 0$ (see the amplitude of approximately 0.1–0.5Hz).

This finding is consistent with the hypothesis presented in Section III-A.

IV. CLOTHING-TYPE MOTION CLASSIFICATION DEVICE

Utilizing the developed sensor and commercially available workwear, we fabricated a wearable sensor device to classify the wearer's activities. We then conducted evaluation experiments to assess the accuracy of the motion classification. The details of the device and the experimental methods are described below.

A. SENSOR DEVICE DETAILS

The sensors were directly sewn onto a workwear jacket and pants (KURODARUMA 32380 and 31380 workwear). As shown in Fig. 7, the workwear is loose-fitting and made of 100% cotton woven fabric, which is not easily stretchable. To prevent the conductive threads from coming into direct contact with the wearer's body during movement, the seams with the conductive threads were sewn on the outside, and insulating fabric tape (Matsuura Industry Co., Ltd.) was applied to the lining (Fig. 7(c-2)). The length L of the attached sensors was set to 100 mm. The angle θ was set to 4.09° ($p = 1.0$ mm, $w = 7.0$ mm), which exhibited the largest change in resistance (based on the experimental results from Section III-C2). These sensors were placed on body parts that are prone to bending deformation during movement. Therefore, the sensors were attached to the olecranons, antecubital fossae, shoulders, armpits, buttocks, hip joints, posterior knees, and anterior knees. The workwear was prepared in two sizes (the jackets in L and LL, and the pants with waist sizes 76 cm and 85 cm), and the sensors were sewn onto the designated parts according to each size.

A custom-built device, consisting of an Arduino (Arduino Mega 2560) and a voltage divider circuit (with the sensor and a resistor connected in series: the sensor resistance approximately 120 Ω, a resistor 270 Ω), was used as the resistance measurement tool for each sensor (Fig. 7(e)). The sensors were connected to the measurement device using integrated circuit (IC) clips. To prevent the IC clips from moving owing to the wearer's motion and introducing noise into the sensor signals, the IC clips were secured to the clothing using Velcro (Fig. 7(c-1)). All sensor data were sampled at 20 Hz, transmitted via USB to a PC, and saved in an Excel file.

B. DEEP LEARNING FOR MOTION CLASSIFICATION

The deep learning model used in this device is a one-dimensional convolutional neural network (1D-CNN). This model was selected because of its ability to extract features from each time step of the time series data and its suitability for low-cost real-time hardware implementation. Since the convolutional filters in a 1D-CNN move only along the time axis, a 1D-CNN can extract features from fixed-length segments. In addition, because of its simple and compact structure that performs only linear 1D convolutions (scalar multiplications and additions), the computational cost is kept low, enabling low-cost real-time hardware implementation [34].

The model consists of two convolutional layers (Conv1D layers). Each layer applies the ReLU activation function and L2 regularization ($\lambda = 0.01$), and includes a dropout layer and a max-pooling layer. The dropout rate is set to 30% to prevent overfitting. The max-pooling layers reduce the dimensions of the feature maps and capture the most prominent features [35]. After the second convolutional layer, a global average pooling layer is added to flatten the feature maps [36], and the output layer employs the softmax activation function. The model is trained using the Adamax optimizer with a learning rate of 1e-4 [37], and the categorical cross-entropy loss function, which is suitable for multiclass classification tasks.

C. MOTION CLASSIFICATION EXPERIMENT

To evaluate the performance of the above-mentioned device and deep learning model, motion data from 10 participants were collected, and based on that data, the movements of

the wearer were classified. The following sections present an overview of the experiment and the accuracy of the motion classification.

1) EXPERIMENTAL SETUP

Ten participants wore the developed wearable sensor device (Fig. 7) and performed 10 activities as shown in Fig. 1. The time-series data of sensor resistance changes measured during these activities were used to train the 1D-CNN for classifying the activities of the wearer. The participants were 10 adult males (height of approximately 167-184 cm, weight of approximately 47-90 kg). The experiment was conducted with the approval of the ethics committee of Shinshu University (Approval No. 387). Regarding the size of the device, each participant wore the size that fits their body type. Each participant's information is summarized in Table 2.

The instructor explained and demonstrated to the participants how to perform the 10 activities. The cycle of the activities was not standardized among the participants. No specific instructions were given to the participants for walking, jogging, and stair climbing. During the walking while carrying a box, each participant carried a box containing a weight equivalent to 20% of their body weight. For the stepping activity, participants were instructed to raise their knees as they would during walking. In the reaching activity, participants moved a pen from a box placed in front of them to another distanced box, and they were instructed to reach with their right hand only. The number of times the participants performed the above mentioned activities was 10 cycles of walking and other moving activities and stepping, 10 steps of ascending and descending stairs, and 10 pens of reaching activities, which are called one set. The participants performed 10 sets of each of the above activities.

2) PREPROCESSING DATA AND EVALUATING MODELS

Concerning data preprocessing, the first step was to normalize the measured sensor resistance values by calculating the percentage change $100\Delta R/R$ (%) from the baseline value R at the start of the measurement. Next, the data for each set was divided using a fixed-width sliding window of 2.5 s with a 50% overlap (50 readings per window) [38], resulting in a total dataset size of 10,320 samples. Finally, the data were filtered using a 6 Hz first-order Butterworth low-pass filter. This filtering step was performed because the frequency spectrum relevant to human movement typically lies within the 0-10 Hz range [39], and it helps to remove noise caused by wrinkles in loose-fitting clothing, thereby enhancing the similarity of signals corresponding to the same movement [13].

The accuracy of the model was evaluated using 5-fold cross-validation, as shown in Fig. 8. The dataset was divided into five folds, each used as the test set in turn, whereas the remaining four folds were split into 70% training data and 30% validation data. The model was trained using these

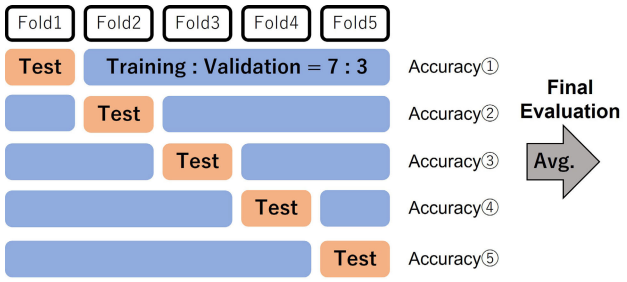

FIGURE 8. K-fold cross-validation (K=5).

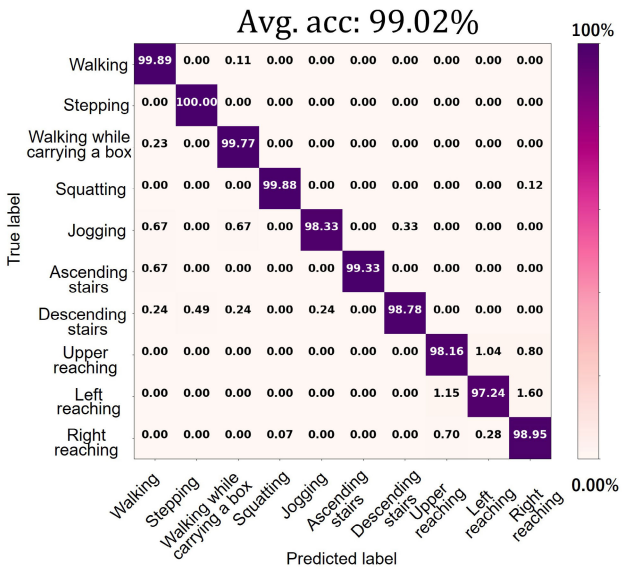

FIGURE 9. Confusion matrix for the classification of 10 types of activities.

splits, and the average accuracy obtained from each training session was used as the final evaluation of the model. During training, the number of epochs was set to 200, and the batch size was 64.

D. EXPERIMENTAL RESULTS

The average accuracy of the activity classification was 99.02% (SD: 0.19) (Fig. 9) after training the model with sensor data (comprising 16 sensors in total) from all participants. Walking, stepping, walking while carrying a box, squatting, and ascending stairs were classified with an accuracy of above 99.3%. Even the lowest accuracy observed for the left-reaching was 97.24%, indicating that all ten types of activities were classified with high accuracy. The high accuracy achieved can be attributed to the sensor's ability to measure the degree and timing of joint flexion according to each activity, as well as the periodicity of the actions (as detailed in Sections IV-D1 and IV-D2).

The accuracy for jogging, descending stairs, and all reaching activities was below 99%, compared to the other activities (e.g., walking) which were classified with accuracy above 99% accuracy. The accuracy for jogging was 98.33%;

TABLE 2. Participant body information and device size data.

Participant	1	2	3	4	5	6	7	8	9	10
Height	182.0 cm	170.1 cm	172.0 cm	172.6 cm	171.7 cm	177.7 cm	167.2 cm	170.4 cm	175.0 cm	184.2 cm
Weight	84.7 kg	55.4 kg	56.5 kg	59.9 kg	59.7 kg	65.2 kg	47.7 kg	56.3 kg	66.0 kg	90.1 kg
BMI	25.57	19.15	19.1	20.11	20.25	20.65	17.06	19.39	21.55	26.55
Jacket size	LL	L	L	L	L	L	L	L	L	LL
Pants size	85 cm	76 cm	76 cm	76 cm	76 cm	76 cm	76 cm	76 cm	76 cm	85 cm

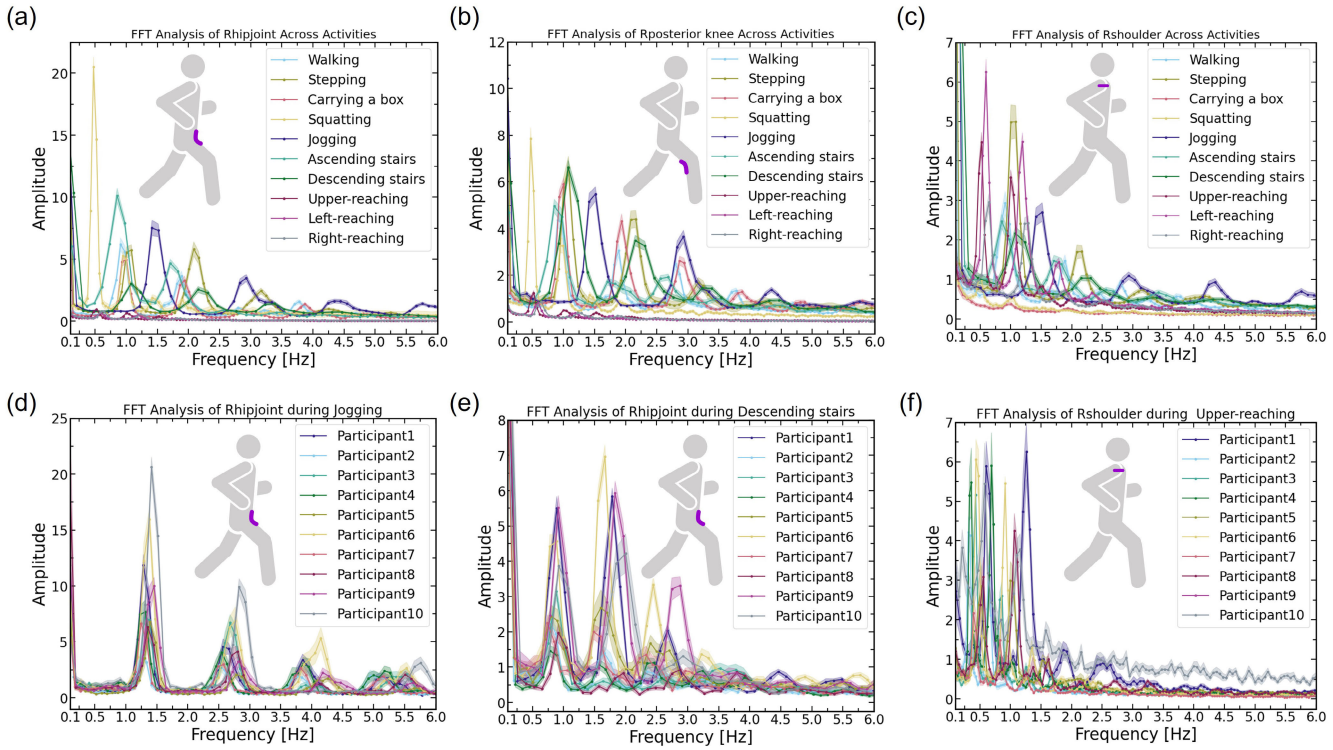

FIGURE 10. Average FFT values of sensor data for each activity across all participants (Right hip joint (a), Right posterior knee (b), Right shoulder (c)). Participant-specific average FFT values of sensor data for each activity (Jogging (d), Descending stairs (e), Upper-reaching (f)).

however, in misclassification cases, it was confused with other activities involving traveling on flat ground, such as walking or walking while carrying a box. The accuracy for descending stairs was 98.78%; however, it was misclassified as stepping with a probability of 0.49%, walking, walking while carrying a box, and jogging with a probability of 0.24%. The causes of these misclassifications mentioned may include the similarity of signals between different activities and variations in signal magnitude and frequency between participants performing the same activity (discussed in Section IV-D3).

1) AMPLITUDE AND FREQUENCY CHARACTERISTICS IN THE FFT OF EACH ACTIVITY DATA

We performed a fast Fourier transform (FFT) on the sensor data from all participants to analyze the classification accuracy. We examined the degree of joint flexion and the movement cycles corresponding to each action. Fig. 10(a) shows a graph of the average values for different activities obtained by performing FFT on the sensor data from the right hip joint of all participants. Note the magnitude of the amplitude between 0.25 Hz and 1.5 Hz in this graph. In the range, the optimal stride frequency for running is reported to be approximately 85–90 strides per minute (approximately 1.42–1.5 Hz) [40], and the activities performed in this experiment did not involve moving the arms and legs at frequencies faster than this. Among the 10 types of activities, the squat activity exhibited the largest amplitude, appearing at 0.47 Hz. Next, the activity of ascending stairs appeared with the second-largest amplitude at 0.85 Hz. The larger amplitudes for these two activities are likely due to greater hip joint flexion compared to the other activities. Walking is characterized by a significant amplitude at 0.91 Hz, stepping at 1.08 Hz, and walking while carrying a box at 1.0 Hz, with only minor amplitude differences. For these activities, the descending stairs activity exhibited a peak amplitude at the same frequency of 1.08 Hz as the stepping activity; however, the amplitude was smaller than that of the previously mentioned activities. This suggests that the descending stairs activity involves less hip joint

flexion than other activities. The jogging activity exhibited a large amplitude at 1.41 Hz, indicating that the hip joint is flexed the fastest. Reaching activities involve minimal lower limb movement, resulting in a small amplitude of approximately 0.5 Hz.

Let us consider the impact of arm movements on the activity classification. Fig. 10(c) shows a graph of the average values for different activities obtained by performing FFT on the sensor data from the right shoulder of all participants. Comparing the peaks in amplitude at approximately 0.5-0.75 Hz for the three types of reaching activities, the order from largest to most minor is left-reaching, upper-reaching, and right-reaching. This is because the sensor bends more significantly as the hand is extended further to the left side relative to the body. During walking, the amplitude peaked at 0.91 Hz because of the swinging arms. In contrast, during walking while carrying a box, the amplitude peak (1.0 Hz) was minimal because the arm motion was relatively fixed. The differences in amplitude and frequency observed in each activity are likely learned by the model as distinguishing features, contributing to the high accuracy in activity classification.

2) ANALYSIS OF JOINT FLEXION TIMING

The timing differences in joint flexion during each activity can be measured from the sensor's time-series data. Fig. 1 (a) shows the time-series data from eight sensors placed on the right side of the body during walking. Focus is placed on the gray painted area of the graph (1.2-1.6 s). In the walking activity, the minima in the sensor signals appear in the order of buttocks (1.2 s), posterior knee (1.4 s), and hip joint (1.6 s). In contrast, the minima appeared at almost the same timing for stepping and ascending stairs activities (Fig. 1 at approximately 1.5 s in (e) and at approximately 1.9 s in (g)). The model can likely learn these timing patterns of joint flexion as activity features, contributing to the high accuracy in activity classification.

3) FACTORS LEADING TO MISCLASSIFICATION OF ACTIVITIES

Fig. 10(b) shows a graph of the average values for different activities obtained by performing FFT on sensor data from the right posterior knees of the participants. In this graph, the focus is placed on the stepping and descending stairs activities. In both cases, a similar amplitude was observed at a frequency of 1.08 Hz. This would have resulted in the most misclassified activity in the data for the stair descending activity and the stepping activity (see Fig. 9).

The amplitude of the sensor signals for each activity varied depending on the participant's BMI, which can result in misclassification with other activities. There was variability in the participants' BMI, with the highest being participant 10, followed by participants 1, 9, and 6 (Table 2). Fig. 10(d, e) shows graphs of the average values for each participant obtained by performing FFT on the sensor data from the right hip joint during jogging and descending stairs. For jogging, the amplitude was between 1.25-1.5 Hz; for descending stairs, the amplitude between 0.75-1.0 Hz varied across participants. For both activities, participants 1, 6, 9, and 10 exhibited larger amplitudes than the other participants. This is because of the differences in BMI between participants. The space between the body and the clothing varies with the participant's physique. Hence, if the joint flexion angle is the same, a more extensive space results in less sensor deformation. Therefore, participants 1, 6, 9, and 10, with higher BMI values (see Table 2) and narrower spaces between their bodies and clothing, likely exhibited larger amplitudes.

The sensor signal frequency during reaching activities varied between participants, which can lead to misclassification with other activities. This is likely because no specific instructions regarding the movement cycle were given to the participants. Fig. 10(f) shows a graph of the average values for each participant obtained by performing FFT on the sensor data from the right shoulder during upward-reaching activity. It can be seen that the frequency at which the amplitude peaks varied between participants, ranging from 0.25 Hz to 1.5 Hz. It is hypothesized that the misclassification of activities is caused by the differences in amplitude and frequency as described above.

V. DISCUSSION

A. PRINCIPLE OF RESISTANCE CHANGE THAT DOES NOT FOLLOW SENSOR CURVATURE VARIATION

Based on the changes in sensor resistance values shown in Section III-C2, it is hypothesized that when this sensor undergoes bending deformation, the resistance values of the bundle section and corner sections' resistance values change in opposite directions, with one increasing and the other decreasing. Therefore, the overall change in sensor resistance ΔR is assumed to be determined by the change in resistance of the bundle section ΔR_{B} and the corner section ΔR_{C}, and can be expressed as follows:

$$\Delta R = \Delta R_{\mathrm{B}} + \Delta R_{\mathrm{C}}. \tag{3}$$

The time difference between the resistance changes ΔR_{B} and ΔR_{C} suggests that even when tensile and compressive strain are applied to the conductive stitching, the resistance may temporarily increase in response to rapid bending deformations, such as during phase transitions in movement. The cases where the sensor curvature is $\varphi > 0$ and $\varphi < 0$ are explained.

1) RESISTANCE CHANGE MECHANISM UNDER TENSILE STRAIN ($\varphi > 0$)

When a tensile strain occurs at the seam on the conductive thread side (Fig. 11(a), when $\varphi > 0$), the conductive path gets shorter at the bundle sections and longer at the corners, and the resistance changes (Fig. 11(a-1), (a-2)). When φ increases, the tension $|\boldsymbol{f}_{\mathrm{T}}|$ increases in the bundle section (Fig. 11(a-2)). This causes the threads to bundle together, shortening the conductive path and reducing ΔR_{B}

(< 0) (red graph in Fig. 11(c)). As φ increases, the contact between threads decreases at the corners owing to tensile strain (Fig. 11(a-1)), the conductive path becomes longer and ΔR_C (>0) increases (red graph in Fig. 11(d)).

Fig. 5(a) shows the experimental values of resistance change with bending deformation of the sensor. The resistance increased and decreased as the curvature of φ increased. Since the resistance increases during the phase transition (Fig. 5(a)), the increase in ΔR_C was considered to be faster than the decrease in ΔR_B.

2) RESUSTANCE CHANGE MECHANISM UNDER COMPRESSION STRAIN ($\varphi < 0$)

When a compressive strain occurs at the seam on the conductive stitch side (Fig. 11(b), when $\varphi < 0$), the conductive path changes at the bundle and corner sections and the resistance changes (Fig. 11(b-1), (b-2)). When φ becomes smaller, the compressive force $|f_C|$ becomes larger in the bundle section (Fig. 11(b-2)). This causes the conductive path to become longer, which leads to an increase in ΔR_B (blue curve in Fig. 11(c)). As φ decreased, the contact between threads increased at corner sections because of compressive strain (Fig. 11(b-1)), and the conductive path became shorter, which in turn decreased ΔR_C (blue curve in Fig. 11(d)).

Fig. 5(b) displays the experimental value of the change in resistance with sensor bending curvature change. The resistance increased and then decreased as the curvature φ decreased. As shown in Section V-A1, ΔR_B increases faster than the decrease in ΔR_C, suggesting that the resistance value increased during the phase transition of the operation.

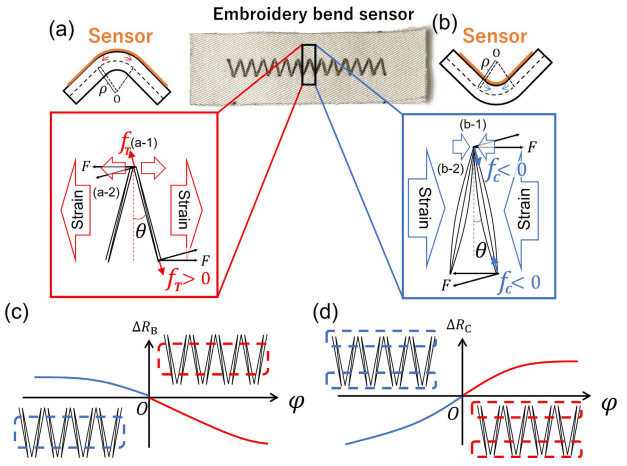

FIGURE 11. Consideration of the principle of resistance change in the bundle and corner sections during bending deformation ((a) $\varphi > 0$, (b) $\varphi < 0$).(c–d) Change in ΔR_B and ΔR_C as φ modifies.

B. SENSOR DEFORMATION ON A GARMENT

When the sensor is attached to a garment, wrinkles with a mixture of convexity ($\varphi > 0$) and concavity ($\varphi < 0$) occur on the sensor in response to the wearer's motion (Fig. 7(d)). By contrast, in the bending experiments discussed in Section III-C, the sensor deformed separately for $\varphi > 0$ and $\varphi < 0$.

The results of the experiment using sensors on a garment in Section IV-D reveal that the sensor resistance commonly showed the same pattern of change for $\varphi > 0$ and $\varphi < 0$, as discussed in Section III-C2. Specifically, the resistance value increased at the start of sensor bending and then decreased. When the sensor bending is resolved, the resistance value increased and then decreased (Fig. 5). Therefore, the resistance value is expected to follow the same pattern even when two bending deformations are mixed.

C. METHODS FOR IMPROVING THE ACCURACY OF THE PROPOSED

Potential strategies to improve the ability of the system to classify finer distinctions in behavior with greater accuracy have been explored. These strategies include increasing the number of sensors, positioning them in optimal locations, and leveraging signal augmentation techniques in conjunction with advanced architectures to capture motion characteristics. The rationales for these approaches are detailed below.

1) IMPACT OF THE NUMBER OF ATTACHED SENSORS ON CLASSIFICATION ACCURACY

By increasing the number of sensors attached to the clothing, it may be possible to classify a greater variety of activities more accurately. Fig. 12 is a confusion matrix showing the classification accuracy of seven types of activities (excluding reaching activities) as the number of sensor data used for training the model increases. The average classification accuracy in this figure shows that the accuracy was 85.96% when only the anterior knee (both legs) sensor data were used for model training. In addition, it was 96.60% when using the anterior knee and buttocks (both legs) sensor data, it was 98.24% when using the anterior knee, buttocks, and hip joint (both legs) sensor data, 99.11% when using all lower body sensors, and it reached 99.61% when using all sensors (including upper body's). This indicates that the average classification accuracy improved as the number of sensors used for training increased.

By training the model with sensor data from multiple body locations, differences in locomotion activities can be classified with high accuracy. The classification accuracy for walking, walking while carrying a box, and ascending stairs was below 90% when using only the anterior knee sensors. This suggests that sensor data from just one location (on both sides) did not fully capture the differences in features among these four activities. By adding sensor data from the buttocks, the classification accuracy improved by 10.45% for walking, 10.45% for walking while carrying a box, and 14.22% and 26.83% for ascending stairs and descending stairs, respectively.

This suggests that increasing the number of sensors makes it possible to learn the degree and timing of joint flexion, which can lead to improved classification and accuracy for a

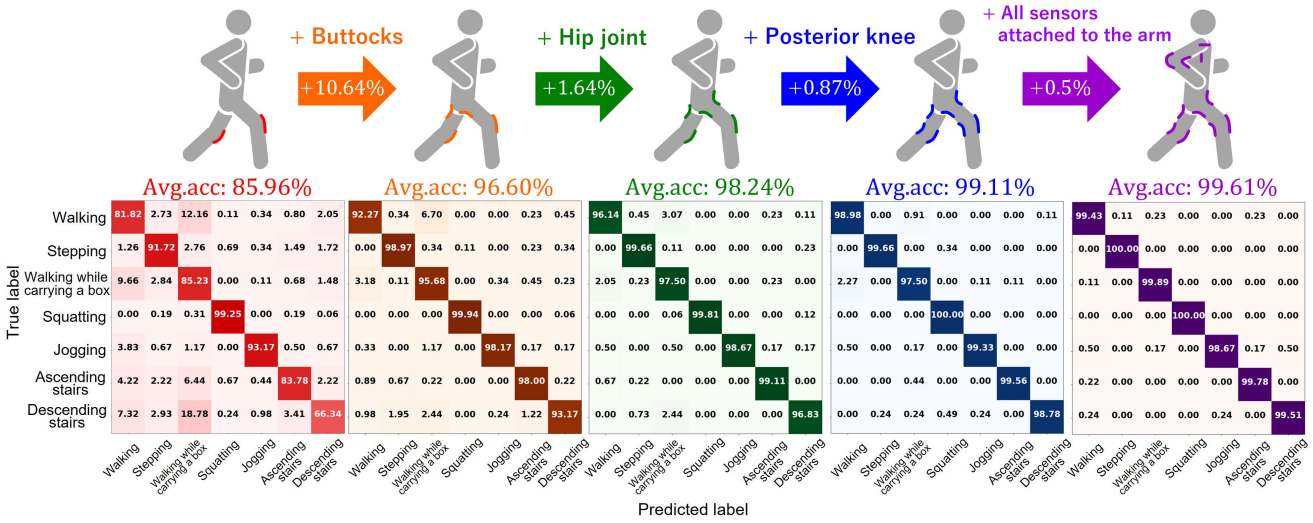

FIGURE 12. Improvement in movement classification accuracy with an increasing number of sensors used for the model training.

more significant number of activities. However, this involves trade-offs, such as higher fabrication cost and reduced user comfort.

2) IMPACT OF SENSOR PLACEMENT DIFFERENCES ON CLASSIFICATION ACCURACY

To improve activity classification accuracy, it is essential to consider the sensor placement that best captures activity differences. Table 3 shows the classification accuracy for seven types of activities when sensors were placed at the hip joint (H), anterior knee (A), posterior knee (P), and buttocks (B) individually, as well as for combinations of these sensors: hip joint and posterior knee (HP), and anterior knee, buttocks, and hip joint (ABH). The highest average classification accuracy was achieved with sensors placed at the hip joint, followed by the posterior knee, buttocks, and anterior knee. Focusing on the classification accuracy for walking and descending stairs, it was observed that the hip joint sensor provided the highest accuracy for walking. In contrast, the posterior knee sensor provided the highest accuracy for descending stairs. This indicates that the hip joint and posterior knee placements contribute significantly to high activity classification accuracy.

It is possible to achieve highly accurate motion classification, even with a limited number of sensors, by strategically placing them in optimal locations. The classification accuracy for HP (using hip joint and posterior knee data) was 98.40%, whereas for ABH (using anterior knee, buttocks, and hip joint data), it was 98.22%, which is lower than that of HP. Thus, exploring appropriate sensor placement could further enhance activity classification accuracy, pushing the boundaries of this technology. Exploration of appropriate sensor placement is described in Section V-C1 in terms of the trade-off between accuracy and increased cost or decreased user comfort.

TABLE 3. Classification accuracy of seven types of activities when training the model with data from sensors individually attached to the hip joint (H), anterior knee (A), posterior knee (P), and buttocks (B), as well as when training with combined data from the hip joint and posterior knee (HP), and from the anterior knee, buttocks, and hip joint (ABH).

	A	B	P	H	HP	ABH
Walking	81.69	79.53	91.41	94.30	95.80	94.59
Stepping	91.68	96.46	95.67	96.61	99.89	99.21
Carrying a box	85.51	89.86	84.64	89.58	95.46	98.74
Squatting	99.24	99.86	99.81	99.74	99.88	99.88
Jogging	93.15	98.72	98.83	98.77	99.33	98.84
Ascending stairs	84.16	96.42	95.84	98.12	98.94	99.33
Descending stairs	66.26	86.48	89.76	87.16	99.50	97.65
Avg. acc	85.96	92.48	93.74	94.90	98.40	98.22

3) SIGNAL ENHANCEMENT AND ADVANCED ARCHITECTURES

The misclassifications observed in this study (e.g., distinguishing between stepping and descending stairs) are likely attributed to the similarity of sensor signals (e.g., posterior knee signals) and participant-specific variations, such as differences in BMI. To address these issues, additional preprocessing techniques, such as band-pass filtering and feature augmentation using frequency-domain characteristics, could potentially reduce signal overlap between activities. Furthermore, employing advanced model architectures, such as LSTM or CNN-LSTM, may enhance the capture of temporal dependencies in the motion data, thereby improving the classification accuracy [13]. Future work will focus on integrating these approaches to reduce misclassification and enhance the overall performance of the system.

D. LIMITATIONS AND FUTURE DIRECTIONS

We evaluated the system using data collected from 10 adult male participants, which may limit the generalizability of the findings. The experimental setup was designed to assess the fundamental performance of the proposed system. However,

demographic variations, such as age, gender, and BMI, could influence sensor signals and classification accuracy (e.g., BMI, as discussed in Section IV-D3). In future studies, we will include participants with more diverse demographics to validate the robustness of the system across broader populations.

We adopted a 5-fold cross-validation approach to evaluate the proposed model. Before splitting the dataset, random shuffling was performed to ensure that each fold contained representative samples. This method minimizes the risk of bias and ensures that the test data in each fold is independent of the training data. However, owing to sliding window segmentation with a 50% overlap, there may be partial redundancy between training and test datasets. To address this limitation, future work will incorporate more rigorous evaluation methods, such as Leave-One-Subject-Out cross-validation.

VI. CONCLUSION

We developed a sewn-type bending sensor created by applying multiple zigzag stitches with conductive thread on the fabric. The sensor was integrated into loose-fitting clothing, and we proposed a system that enables motion classification of the wearer by training the collected data using deep learning. The proposed method was evaluated by measuring data from 10 participants performing 10 different locomotion and reaching activities. As a result, the system demonstrated high performance, achieving an average classification accuracy of 99.02% for the 10 activities. Furthermore, by optimizing the number and placement of sensors, there is potential to classify a greater variety of activities and detect subtle differences in physical actions.

The proposed system has demonstrated significant potential for applications across various fields. In healthcare, it can monitor rehabilitation progress, detect fall risks in elderly individuals, and support physical therapy. In the sports sector, the system can analyze movements of athletes to provide insights for performance enhancement. It can also monitor the postures of workers and detect hazardous movements in industrial settings. Moreover, the system offers a practical and scalable solution for everyday wearable applications by enabling motion classification with loose-fitting garments.

The future prospect involves verifying whether the proposed method can classify the movements of unmeasured individuals and perform personal authentication. Furthermore, we aim to optimize the number and placement of sensors to enable more accurate detection of subtle movement differences.

REFERENCES

[1] C. Buckley, L. Alcock, R. McArdle, R. Rehman, S. D. Din, C. Mazzà, A. Yarnall, and L. Rochester, "The role of movement analysis in diagnosing and monitoring neurodegenerative conditions: Insights from gait and postural control," *Brain Sci.*, vol. 9, no. 2, p. 34, Feb. 2019.

[2] S. Patel, H. Park, P. Bonato, L. Chan, and M. Rodgers, "A review of wearable sensors and systems with application in rehabilitation," *J. NeuroEng. Rehabil.*, vol. 9, no. 1, pp. 1–17, Dec. 2012.

[3] J. Ahn, J. Park, S. S. Lee, K.-H. Lee, H. Do, and J. Ko, "SafeFac: Video-based smart safety monitoring for preventing industrial work accidents," *Expert Syst. Appl.*, vol. 215, Apr. 2023, Art. no. 119397.

[4] N. Bidargaddi, A. Sarela, L. Klingbeil, and M. Karunanithi, "Detecting walking activity in cardiac rehabilitation by using accelerometer," in *Proc. 3rd Int. Conf. Intell. Sensors, Sensor Netw. Inf.*, Dec. 2007, pp. 555–560.

[5] H. M. Thang, V. Q. Viet, N. Dinh Thuc, and D. Choi, "Gait identification using accelerometer on mobile phone," in *Proc. Int. Conf. Control, Autom. Inf. Sci. (ICCAIS)*, Nov. 2012, pp. 344–348.

[6] H. T. Butt, M. Pancholi, M. Musahl, P. Murthy, M. A. Sanchez, and D. Stricker, "Inertial motion capture using adaptive sensor fusion and joint angle drift correction," in *Proc. 22th Int. Conf. Inf. Fusion (FUSION)*, Jul. 2019, pp. 1–8.

[7] H. Harm, O. Amft, D. Roggen, and G. Tröster, "SMASH: A distributed sensing and processing garment for the classification of upper body postures," in *Proc. 3rd Int. ICST Conf. Body Area Netw.*, 2008, pp. 1–16.

[8] S. Sarangi, S. Sharma, and B. Jagyasi, "Agricultural activity recognition with smart-shirt and crop protocol," in *Proc. IEEE Global Humanitarian Technol. Conf. (GHTC)*, Oct. 2015, pp. 298–305.

[9] G. Loke, T. Khudiyev, B. Wang, S. Fu, S. Payra, Y. Shaoul, J. Fung, I. Chatziveroglou, P.-W. Chou, I. Chinn, W. Yan, A. Gitelson-Kahn, J. Joannopoulos, and Y. Fink, "Digital electronics in fibres enable fabric-based machine-learning inference," *Nature Commun.*, vol. 12, no. 1, p. 3317, Jun. 2021.

[10] Y. Koyama, M. Nishiyama, and K. Watanabe, "Physical activity recognition using hetero-core optical fiber sensors embedded in a smart clothing," in *Proc. IEEE 7th Global Conf. Consum. Electron. (GCCE)*, Oct. 2018, pp. 71–72.

[11] A. Kiaghadi, M. Baima, J. Gummeson, T. Andrew, and D. Ganesan, "Fabric as a sensor: Towards unobtrusive sensing of human behavior with triboelectric textiles," in *Proc. 16th ACM Conf. Embedded Networked Sensor Syst.*, Nov. 2018, pp. 199–210.

[12] L. Wang, T. Gu, X. Tao, and J. Lu, "Toward a wearable RFID system for real-time activity recognition using radio patterns," *IEEE Trans. Mobile Comput.*, vol. 16, no. 1, pp. 228–242, Jan. 2017.

[13] Q. Lin, S. Peng, Y. Wu, J. Liu, W. Hu, M. Hassan, A. Seneviratne, and C. H. Wang, "E-jacket: Posture detection with loose-fitting garment using a novel strain sensor," in *Proc. 19th ACM/IEEE Int. Conf. Inf. Process. Sensor Netw. (IPSN)*, Apr. 2020, pp. 49–60.

[14] Y. Cha, H. Kim, and D. Kim, "Flexible piezoelectric sensor-based gait recognition," *Sensors*, vol. 18, no. 2, p. 468, Feb. 2018.

[15] H. Bello, B. Zhou, S. Suh, and P. Lukowicz, "MoCapaci: Posture and gesture detection in loose garments using textile cables as capacitive antennas," in *Proc. Int. Symp. Wearable Comput.*, Sep. 2021, pp. 78–83.

[16] C. Mattmann, O. Amft, H. Harms, G. Troster, and F. Clemens, "Recognizing upper body postures using textile strain sensors," in *Proc. 11th IEEE Int. Symp. Wearable Comput.*, Oct. 2007, pp. 29–36.

[17] X. Li, H. Hu, T. Hua, B. Xu, and S. Jiang, "Wearable strain sensing textile based on one-dimensional stretchable and weavable yarn sensors," *Nano Res.*, vol. 11, no. 11, pp. 5799–5811, Nov. 2018.

[18] M. I. M. Esfahani and M. A. Nussbaum, "Classifying diverse physical activities using 'smart garments,'" *Sensors*, vol. 19, no. 14, p. 3133, 2019.

[19] P. T. Gibbs and H. Asada, "Wearable conductive fiber sensors for multi-axis human joint angle measurements," *J. NeuroEngineering Rehabil.*, vol. 2, no. 1, pp. 1–18, Mar. 2005.

[20] R. Ramalingame, R. Barioul, X. Li, G. Sanseverino, D. Krumm, S. Odenwald, and O. Kanoun, "Wearable smart band for American sign language recognition with polymer carbon nanocomposite-based pressure sensors," *IEEE Sensors Lett.*, vol. 5, no. 6, pp. 1–4, Jun. 2021.

[21] B. Zhou, M. Sundholm, J. Cheng, H. Cruz, and P. Lukowicz, "Measuring muscle activities during gym exercises with textile pressure mapping sensors," *Pervas. Mobile Comput.*, vol. 38, pp. 331–345, Jul. 2017.

[22] B. Osoinach, "Proximity capacitive sensor technology for touch sensing applications," *Freescale White Paper*, vol. 12, pp. 1–12, Feb. 2007.

[23] P. Parzer, F. Perteneder, K. Probst, C. Rendl, J. Leong, S. Schuetz, A. Vogl, R. Schwoediauer, M. Kaltenbrunner, S. Bauer, and M. Haller, "RESi: A highly flexible, pressure-sensitive, imperceptible textile interface based on resistive yarns," in *Proc. 31st Annu. ACM Symp. User Interface Softw. Technol.*, Oct. 2018, pp. 745–756.

[24] R. Aigner, A. Pointner, T. Preindl, P. Parzer, and M. Haller, "Embroidered resistive pressure sensors: A novel approach for textile interfaces," in *Proc. CHI Conf. Hum. Factors Comput. Syst.*, Apr. 2020, pp. 1–13.

[25] J. Meyer, P. Lukowicz, and G. Troster, "Textile pressure sensor for muscle activity and motion detection," in *Proc. 10th IEEE Int. Symp. Wearable Comput.*, Oct. 2006, pp. 69–72.
[26] A. Vogl, P. Parzer, T. Babic, J. Leong, A. Olwal, and M. Haller, "StretchEBand: Enabling fabric-based interactions through rapid fabrication of textile stretch sensors," in *Proc. CHI Conf. Hum. Factors Comput. Syst.*, New York, NY, USA, May 2017, pp. 2617–2627.
[27] O. Tangsirinaruenart and G. Stylios, "A novel textile stitch-based strain sensor for wearable end users," *Materials*, vol. 12, no. 9, p. 1469, May 2019.
[28] B. Greenspan, M. L. Hall, H. Cao, and M. A. Lobo, "Development and testing of a stitched stretch sensor with the potential to measure human movement," *J. Textile Inst.*, vol. 109, no. 11, pp. 1493–1500, Nov. 2018.
[29] L. E. Dunne, G. Gioverto, J. Coughlin, and K. Bibeau, "Machine-stitched E-textile stretch sensors," *Sensors Transducers*, vol. 202, pp. 25–37, Jan. 2013.
[30] G. Gioberto, "Garment-integrated wearable sensing for knee joint monitoring," in *Proc. ACM Int. Symp. Wearable Comput., Adjunct Program*, Sep. 2014, pp. 113–118.
[31] G. Gioberto, J. Coughlin, K. Bibeau, and L. E. Dunne, "Detecting bends and fabric folds using stitched sensors," in *Proc. Int. Symp. Wearable Comput.*, Sep. 2013, pp. 53–56.
[32] K. Minami, Y. Akiyama, and T. Umedachi, "Embroidery bend sensor of multiple zigzag stitch for motion classification in loose-fitting garments," in *Proc. JSME Conf. Robot. Mechatronics*, Utsunomiya, Japan, Jun. 2024, pp. 1–10.
[33] K. Shinoda, D. A. Chacon, and K. Yatani, "An embroidery touch sensor with layered structure of conductive and nonconductive threads," *IEEE Sensors Lett.*, vol. 7, no. 6, pp. 1–4, Jun. 2023.
[34] S. Kiranyaz, T. Ince, O. Abdeljaber, O. Avci, and M. Gabbouj, "1-D convolutional neural networks for signal processing applications," in *Proc. IEEE Int. Conf. Acoust., Speech Signal Process. (ICASSP)*, May 2019, pp. 8360–8364.
[35] H. Gholamalinezhad and H. Khosravi, "Pooling methods in deep neural networks, a review," 2020, *arXiv:2009.07485*.
[36] M. Lin, Q. Chen, and S. Yan, "Network in network," 2013, *arXiv:1312.4400*.
[37] D. P. Kingma and J. Ba, "Adam: A method for stochastic optimization," 2014, *arXiv:1412.6980*.
[38] D. Anguita, A. Ghio, L. Oneto, X. Parra, and J. L. Reyes-Ortiz, "A public domain dataset for human activity recognition using smartphones," in *Proc. Eur. Symp. Artif. Neural Netw.*, Jan. 2013, pp. 437–442.
[39] J. Lester, B. Hannaford, and G. Borriello, "'Are you with me?'—Using accelerometers to determine if two devices are carried by the same person," in *Proc. Int. Conf. Pervasive Comput.* Cham, Switzerland: Springer, 2004, pp. 33–50.
[40] D. E. Lieberman, A. G. Warrener, J. Wang, and E. R. Castillo, "Effects of stride frequency and foot position at landing on braking force, hip torque, impact peak force and the metabolic cost of running in humans," *J. Exp. Biol.*, vol. 218, no. 21, pp. 3406–3414, Nov. 2015.

KAISEI MINAMI received the B.S. degree from the Faculty of Textile Science and Technology, Shinshu University, Nagano, Japan, in 2023, where he is currently pursuing the master's degree.

His research interests include developing sensors fabricated using conductive threads and developing wearable devices using these sensors.

YASUHIRO AKIYAMA (Member, IEEE) received the B.E. degree in engineering from Tokyo Institute of Technology, Tokyo, Japan, in 2006, and the M.S. and Ph.D. degrees in engineering from The University of Tokyo, Tokyo, in 2008 and 2011, respectively. He was an Assistant Professor with Nagoya University, Japan, until 2021. He is currently an Associate Professor with Shinshu University, Japan. His main research interests include mechanical safety, human–robot interaction, and break manned space mission.

TAKUYA UMEDACHI received the B.E. and M.S. degrees in engineering from Nagoya University, Japan, in 2003 and 2005, respectively, and the Ph.D. degree in engineering from Tohoku University, Miyagi, in 2009. He has been a Research Fellow with Japan Society for the Promotion of Science (PD), Department of Mathematical and Life Sciences, Hiroshima University, from 2012 to 2016. He was with the Department of Biology, Tufts University, from 2012 to 2016. He was a Project Lecturer with the Graduate School of Information Science and Technology, The University of Tokyo, Japan, from 2016 to 2019. He is currently an Associate Professor with Shinshu University, Japan. His main research interests include bio-inspired soft robotics and autonomous decentralized systems.